Available online at www.sciencedirect.com
ScienceDirect
Journal of Solid State Chemistry 180 (2007) 75–83
JOURNAL OF SOLID STATE CHEMISTRY
www.elsevier.com/locate/jssc

Synthesis and properties of the double perovskites La_2NiVO_6, La_2CoVO_6, and La_2CoTiO_6

K.L. Holman[a,*], Q. Huang[b], T. Klimczuk[c], K. Trzebiatowski[c], J.W.G. Bos[a], E. Morosan[a], J.W. Lynn[b], R.J. Cava[a]

[a]*Department of Chemistry, Princeton University, Princeton, NJ 08544, USA*
[b]*NIST Center for Neutron Research, National Institute of Standards and Technology, Gaithersburg, MD 20899, USA*
[c]*Faculty of Applied Physics and Mathematics, Gdansk University of Technology, Narutowicza 11/12, 80-952 Gdansk, Poland*

Received 2 June 2006; received in revised form 11 September 2006; accepted 12 September 2006
Available online 1 October 2006

Abstract

The double perovskites La_2CoVO_6, La_2CoTiO_6, and La_2NiVO_6, are described. Rietveld fitting of neutron and powder X-ray diffraction data show La_2NiVO_6 and La_2CoVO_6 to have a disordered arrangement of B-cations whereas La_2CoTiO_6 shows ordering of the B-cations (with ~5% Co/Ti inversion). Curie–Weiss fits to the linear region of the $1/\chi$ plots reveal Weiss temperatures of −107, −34.8, and 16.3 K for La_2CoVO_6, La_2CoTiO_6, and La_2NiVO_6, respectively, and magnetic transitions are observed. La_2CoTiO_6 prepared by our method differs from material prepared by lower-temperature routes. A simple antiferromagnetic spin model is consistent with the data for La_2CoTiO_6. These compounds are semiconductors with bandgaps of 0.41 (La_2CoVO_6), 1.02 (La_2CoTiO_6) and 0.45 eV (La_2NiVO_6).

Keywords: Double perovskite; La_2CoVO_6; La_2CoTiO_6; La_2NiVO_6; Semiconductor; Neutron diffraction; Antiferromagnetism

1. Introduction

Perovskites show a variety of properties ranging from superconductivity in $BaBi_{1-x}Pb_xO_3$, [1] to colossal magnetoresistance in $La_{1-x}Ca_xMnO_3$, [2] to ferroelectricity in $BaTiO_3$ [3]. The ideal ABO_3 perovskite is a corner-sharing cubic network of BO_6 octahedra with A cations occupying the 12 coordinate position between 8 BO_6 octahedra. If two atoms, B′ and B″, are placed on the B sublattice, a double perovskite is formed with the general formula $A_2B'B''O_6$. The two B atoms can be randomly mixed, like Ni and Co in La_2NiCoO_6, [4] or they can order, causing a change in the symmetry and periodicity [5,6]. Ordering can be in a rock salt pattern with different cations occupying alternating BO_6 octahedra, like Sr_2CoUO_6, [7] or, rarely, it can form layers of alternating B cations, like La_2CuSnO_6 [8,9]. Ordering of the B cations occurs when there is either a large size dissimilarity, like Rh^{3+} and Ta^{5+} in Sr_2RhTaO_6 [6] or when the charge difference is greater than 2, like Mn^{2+} and Nb^{5+} in $LaCaMnNbO_6$ [5,8].

Double perovskites have shown promise in the development of spin polarized conduction and ferromagnetic semiconductors. Recently, La_2NiMnO_6 has been reported to display ferromagnetism near room temperature as well as to exhibit semiconducting properties. [10] Here we report two new double perovskites: La_2NiVO_6 and La_2CoVO_6, and further characterize La_2CoTiO_6, which has been previously reported: the synthetic conditions employed for this compound impact the B-site mixing and magnetic properties [11,12]. La_2NiVO_6 displays weak ferromagnetic interactions while La_2CoVO_6 and La_2CoTiO_6 show antiferromagnetic interactions. La_2NiVO_6, La_2CoVO_6, and La_2CoTiO_6 are semiconductors with bandgaps of 0.45, 0.41, and 1.02 eV, respectively.

2. Experimental

Polycrystalline samples were prepared by combining TiO_2 or a combination of VO_2 and V_2O_3 with prereacted

*Corresponding author. Fax: +1 609 258 6746.
E-mail address: kholman@princeton.edu (K.L. Holman).

0022-4596/$ - see front matter © 2006 Elsevier Inc. All rights reserved.
doi:10.1016/j.jssc.2006.09.013

$La_2NiO_{4+\delta}$ or $La_2CoO_{4+\delta}$. $La_2NiO_{4+\delta}$ and $La_2CoO_{4+\delta}$ were synthesized by standard solid state methods from La_2O_3 (Rare Earth Products, 99.99%) and NiO (Alfa, 99.998%) or CoO (Alfa, 95%). La_2O_3 was dried at 900 °C in air overnight to remove water and CO_2. Powders were ground, pressed into pellets, and heated at 1250 °C under flowing N_2 for 48 h with 3 intermediate grindings. This synthesis method produced the desired pure $La_2NiO_{4+\delta}$ and $La_2CoO_{4+\delta}$, but both precursors contained a small amount (less than 1%) of excess oxygen. In the case of $La_2NiO_{4+\delta}$, the excess oxygen was removed, as previously reported, [13] by heating for 1 h at 375°C under flowing 5% H_2 in Argon. Powder X-ray diffraction was used to confirm the purity of these precursors. The resulting patterns matched previously reported X-ray data allowing determination of the excess oxygen content [14,15].

La_2NiO_4 and $La_2CoO_{4+\delta}$ were then combined with stoichiometric amounts of TiO_2 (Alfa 99.8%), VO_2 (Cerac 99.5%), and V_2O_3 (Alfa 99.5%) with the ratio of the vanadium oxides picked to balance any excess oxygen found in the precursors. The powders were ground, pelletized, placed in a dense alumina crucible, and sealed in an evacuated quartz tube. The tubes were then fired at 1175 °C for 10 days. After this step, La_2CoVO_6 and La_2CoTiO_6 were found to be pure, but for La_2NiVO_6, arc melting was used to complete the synthesis.

Purity and structure of the final product were determined by powder XRD using CuKα radiation. The neutron powder diffraction data for the three compounds were collected at room temperature using the BT-1 beamline at the NIST Center for Neutron Research, on a high-resolution powder neutron diffractometer, with monochromatic neutrons of wavelength 1.5403 Å produced by a Cu(311) monochromator. Additional data for La_2CoTiO_6 was collected at 4 K and with a monochromic wavelength of 2.0783(2) Å produced by a Ge(311) monochromator. Collimators with horizontal divergences of 7′, 15′, and 20′ of arc were used after the sample, and before and after the monochromator, respectively. Data were collected in the 2θ range of 3° and 168°, with a step size of 0.05′. The structural parameters were refined using the program, GSAS [16], with the user interface, EXPGUI [17]. The neutron scattering amplitudes used in the refinement were 0.824, 1.03, 0.249, −0.0382, −0.344 and 0.581 (10^{-12} cm) for La, Ni, Co, V, Ti and O, respectively.

Zero field cooled (ZFC) magnetic susceptibilities of the samples were collected on a Quantum Design PPMS in a 1 T field from 5 to 250 K unless otherwise stated. Magnetic characterization was performed by fitting the χ vs. T data to the Curie–Weiss Law in the form $\chi(T) = \chi_0 + (C/(T-\theta))$, where χ_0 is a temperature independent contribution to the susceptibility. Resistivity measurements for La_2NiVO_6, La_2CoVO_6, and La_2CoTiO_6 were made by a two probe method, which was suitable due to the high resistances of the samples. Bars of each sample were cut and connected to two gold wires with silver epoxy. The resistivity of each sample was measured under a 20 mTorr vacuum from 400 °C to room temperature.

3. Results

3.1. Crystal structure

In order to determine whether or not the B cations are ordered, only the neutron powder diffraction data were used in structural refinements. Since the neutron scattering amplitudes between Ni and V, Co and V, and Co and Ti are significantly different, the site occupancies can be readily identified. Refinements show that the structure of La_2NiVO_6 and La_2CoVO_6 can be well described with an orthorhombic space group *Pnma* (#62). In this model, there is only one crystallographic site 4*b* $(0,0,\frac{1}{2})$ for B cations, i.e. the symmetry does not allow for an ordered arrangement of the B cations. A model with space group symmetry $P2_1/n$ (#14), a subgroup of *Pnma*, was also tested. The 4*b* $(0,0,\frac{1}{2})$ site in *Pnma* can be separated into two independent crystallographic sites, 2*d* $(\frac{1}{2},0,0)$ and 2*c* $(\frac{1}{2},0,\frac{1}{2})$, in $P2_1/n$ that will allow an ordered arrangement for the B cations. Since the neutron scattering amplitude for V is very close to 0, only occupancies for Ni and Co at the 2*d* and 2*c* sites were varied in La_2NiVO_6 and La_2CoVO_6. Refinement results indicated that the occupancy parameters at the two possible B sites are very close, suggesting that the transition metals were not ordered. Therefore, the symmetry *Pnma* was used in the final structure calculations for La_2NiVO_6 and La_2CoVO_6. Figs. 1A and B show the observed, calculated, and difference plots for these two compounds at room temperature. For La_2CoTiO_6, the best fit, as shown in the inset of Fig. 1C, was obtained using the ordered model with $P2_1/n$ symmetry in which the Co and Ti occupy the 2*d* and 2*c* sites, respectively. Although the reduced χ^2 values for the disordered model in *Pnma* and the ordered model in $P2_1/n$ were similar, the ordered model was determined to be correct because of the fits of the first peak in the observed pattern as shown in the inset of Fig. 1C. Refinements revealed small amounts of intermixing (~5%) of Co and Ti on the B and B′ sites. The refinements show that the higher-temperature synthesis (1300 °C) method gives more complete B site ordering than was found for the lower-temperature synthesis is temperature (900 °C) method previously reported. [12] A summary of the refined structural data for these materials is given in Table 1. The refined formulae are $La_2Ni_{1.04}V_{.96}O_6$, $La_2Co_{1.10}V_{.80}O_6$, and La_2CoTiO_6. Because the refined unit cell results in a β angle that is approximately 90°, $LaCoTiO_6$ can be regarded dimensionally as nearly orthorhombic; the main factor driving the monoclinic symmetry is the ordering of the B′ and B″ cations.

All three compounds have perovskite tolerance factors close to but below unity; 0.96 for La_2CoTiO_6, 0.97 for La_2CoVO_6 and 0.96 for La_2NiVO_6. These tolerance factors are sufficient to lead to tilting of the BO_6 and $B'O_6$ octahedra and the neutron and X-ray data confirms this. In the Glazer notation for octahedral tilting, [18,19] the angle of rotation about each of the Cartesian axes is noted with a symbol and a superscript above each to signify whether the

next layer along the rotation axis rotates in the same (+) or opposite (−) direction [18]. The tilt system for all three compounds is $a^+b^-b^-$, indicating that the rotation angle around the x-axis is not equal to the rotation around the y and z-axes [6,19]. The octahedral tilts are often calculated from the B–O–B bond angles (δ) as $((180-\delta)/2)$ and are given in Table 1. Transition metal–oxygen bond lengths for the three compounds are also shown in Table 1.

3.2. Magnetic properties

The susceptibility vs. temperature data for La_2NiVO_6, La_2CoVO_6, and La_2CoTiO_6 are presented in Figs. 3, 4, and 5, respectively. All compounds are paramagnetic above 75 K and obey the Curie–Weiss law. The effective overall moment (p_{eff}), Weiss constant (θ_W) and temperature independent term (χ_0) calculated from the fitted data are presented in Table 2. The broad peaks in the susceptibility data for La_2NiVO_6 and La_2CoVO_6, indicating diffuse ordering transitions, are consistent with a disordered B-site distribution, while the relatively sharp peak in the susceptibility data of La_2CoTiO_6 is consistent with B-site ordering.

La_2NiVO_6 shows a ferromagnetic intercept in the $1/\chi$ vs. T plot (Fig. 3). A Curie–Weiss fit gives a $\theta_W = 16.3$ K, indicating weak ferromagnetic interactions. The paramagnetic moment is 2.34 μ_B/f.u, which is lower than expected from the sum of the Ni and V cation moments, as we expect the Ni to be in the 2+ state with a moment of 3.2 μ_B/Ni^{2+} [20] and the V to be in the 4+ state with a

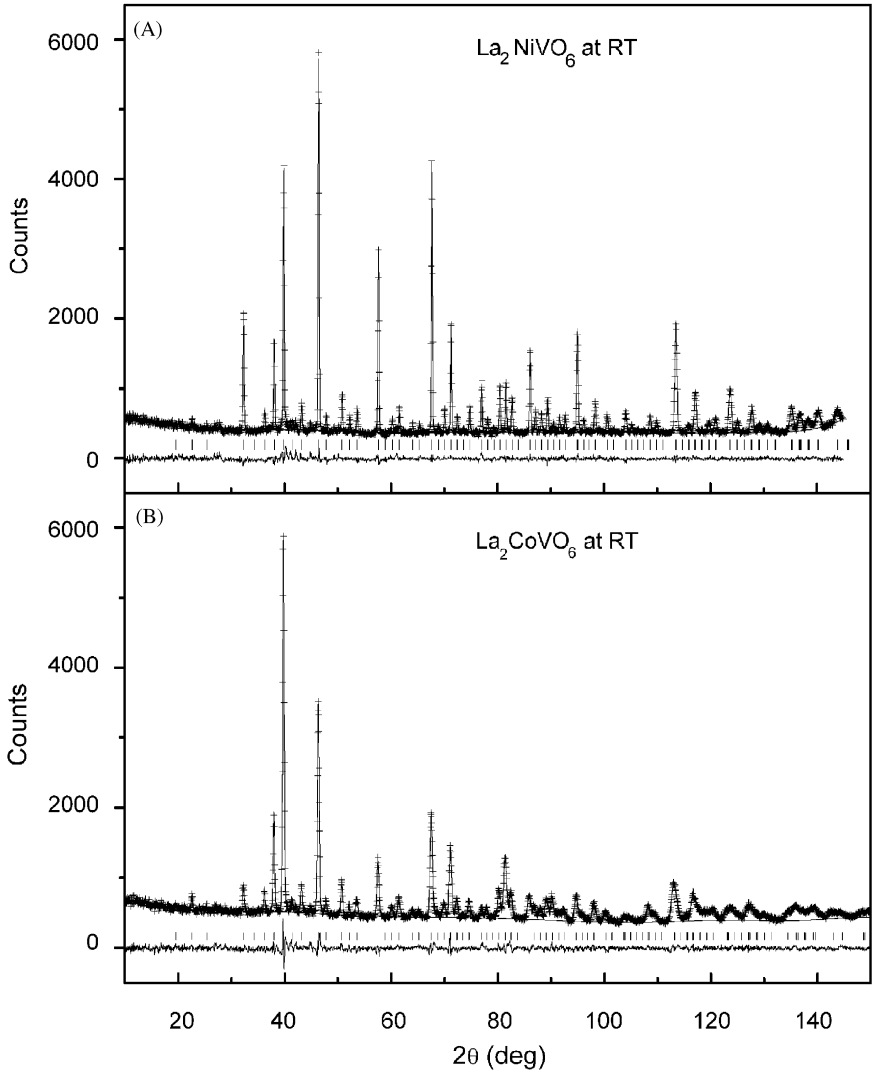

Fig. 1. Plots of observed (crosses) and calculated (solid line) neutron powder diffraction intensities. The vertical lines show the possible Bragg peak positions and the differences between observed and calculated intensities are shown at the bottom of each plot. Upper vertical hatch marks below data in main panel indicate positions of reflections for magnetic cell; lower vertical hatch marks indicate positions of reflections for crystallographic cell. (A) La_2NiVO_6 in the *Pnma* space group at RT. (B) La_2CoVO_6 in the *Pnma* space group at RT. (C) La_2CoTiO_6 in the $P2_1/n$ space group at RT. The inset on the left is a portion of the pattern fit by *Pnma* symmetry, in which the (0 1 1) peak at ~19.5° was not fit well, and the inset on the right plot shows a significantly improved fit by using the monoclinic $P2_1/n$ ordered model. (D) La_2CoTiO_6 at 4 K in the $P2_1/n$ space group. The magnetic intensities were fit very well, as shown in the inset the for low angle portion of the pattern, where magnetic peaks were indexed by a superstructure lattice $a \times 2b \times 2c$.

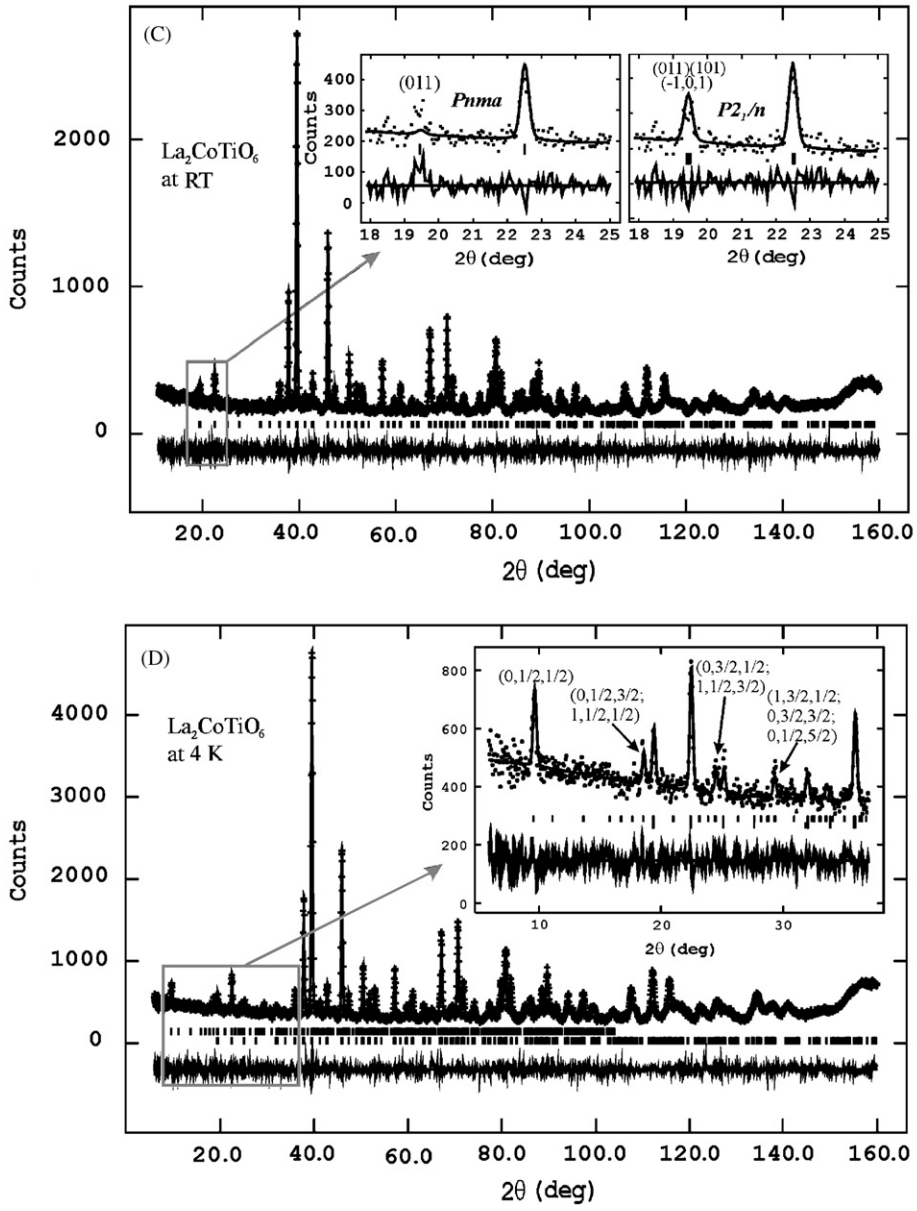

Fig. 1. (*Continued*)

moment of $1.8\,\mu_B/V^{4+}$ [20]. The reason for this is not known. The M vs. H loop (Fig. 2) shows no hysteresis at 5 K or 240 K. At 5 K, the data remain Brillouin like at fields up to 5 T, further indication that ferromagnetic interactions are weak. Comparison of zero field cooled and field cooled magnetic susceptibility data for La_2NiVO_6 does not show the presence of a spin glass transition.

La_2CoVO_6 shows antiferromagnetic behavior in the 1 T, χ vs. T plot (Figs. 3 and 4 inset), with one major broad feature in the data at 11.8 K and another minor one at 51.2 K. The $1/\chi$ data (Fig. 4) gives a θ_W of -107.2 K, indicating antiferromagnetic interactions. La_2CoVO_6 has an overall moment of $5.34\,\mu_B$/f.u., determined from the Curie constant. This is consistent with Co having $S = 3/2$ in the 2+ high spin state with an expected value of $4.8\,\mu_B/Co^{2+}$ while V has $S = 1/2$ in the +4 state ($1.8\,\mu_B/V^{4+}$) [20]. The broad susceptibility features, around 50 and 14.8 K, found in the χ vs. T data at 1 T of La_2CoVO_6 suggested that an investigation of the changes of the susceptibility with field would be of interest. The behavior of the χ vs. T data for La_2CoVO_6 in applied fields varying from 0.1 to 5 T is shown in Fig. 5. The lower temperature peak at 27 K in the 0.1 T field shifts to lower temperatures and broadens with increasing field. The weak high temperature feature near 50 K did not shift with increased field but became better defined. To study these features in more detail, the peak locations, after the data had undergone 5-point smoothing, were identified by a two peak Gaussian fit to the smoothed data. The inset of Fig. 5 shows a general phase diagram whose data points show the temperature of the lower temperature peak maximum as a function of field. The weak high temperature feature is

Table 1
Lattice parameters and atomic positions of $A_2B'B''O_6$ at room temperature and 4 K as determined by neutron diffraction

	La_2NiVO_6	La_2CoVO_6	La_2CoTiO_6	
	RT[a]	RT[b]	RT[c]	4 K[d]
Space group	*Pnma*	*Pnma*	$P2_1/n$	$P2_1/n$
a (Å)	5.52182(29)	5.5402(8)	5.5703(6)	5.5598(5)
b (Å)	7.80614(26)	7.8247(10)	5.5954(5)	5.5920(5)
c (Å)	5.52584(34)	5.5429(7)	7.8797(7)	7.8622(7)
β			89.955(11)	89.968(10)
La position	4c	4c	4e	4e
x	0.0295(4)	0.0318(5)	0.5073(10)	0.5070(7)
y	0.2500	0.25000	0.5336(4)	0.53677(28)
z	0.0067(8)	0.0125(8)	0.2478(13)	0.2502(9)
U*100 (Å^2)	1.25(4)	1.08(7)	0.94(5)	0.40(4)
B′ position	4b	4b	2d	2d
x	0.0000	0.00000	0.50000	0.50000
y	0.0000	0.00000	0.00000	0.00000
z	0.5000	0.50000	0.00000	0.00000
U*100(Å^2)	0.50(6)	1.04(33)	0.07(29)	0.09(18)
Frac.Occ.	0.524(5)	0.553(18)	0.891(17)/0.109(17)*	0.950(9)/0.050(9)*
B″ position	4b	4b	2c	2c
x	0.0000	0.00000	0.00000	0.00000
y	0.0000	0.00000	0.50000	0.50000
z	0.5000	0.50000	0.00000	0.00000
U*100 (Å^2)	0.41(8)	1.04(33)	0.07(29)	0.09(18)
Frac. Occ	0.476(5)	0.447(18)	0.109(17)/0.891(17)*	0.050(9)/0.950(9)*
O(1) position	4c	4c	4e	4e
O(1) *x*	0.4894(7)	0.4905(8)	0.2992(16)	0.2950(11)
O(1) *y*	0.250000	0.25000	0.7175(19)	0.7203(10)
O(1) *z*	−0.0708(9)	−0.0793(12)	−0.0365(10)	−0.0358(9)
U*100 (Å^2)	1.24(7)	1.25(9)	1.30(5)	0.88(4)
O(2) position	8d	8d	4e	4e
O(2) *x*	0.2818(6)	0.2809(7)	0.4239(12)	0.4247(7)
O(2) *y*	0.0361(4)	0.0350(5)	0.9840(8)	0.9838(5)
O(2) *z*	0.2826(5)	0.2854(6)	0.2493(12)	0.2482(10)
U*100 (Å^2)	1.17(5)	1.61(9)	1.30(5)	0.88(4)
O(3) position			4e	4e
O(3) *x*			0.2263(15)	0.2203(10)
O(3) *y*			0.2090(19)	0.2023(11)
O(3) *z*			−0.0434(10)	0.0454(9)
U*100 (Å^2)			1.30(5)	0.88(4)
Tilt angle θ	10.96(7)	10.9(1)	12.2(2)	11.7(2)
Tilt angle φ	11.47(16)	12.75(2)	12.4(3)	12.3(2)
B–O(1)	1.986(4)	1.978(4)		
B–O(1)	1.9925(33)	2.013(4)		
B–O(2)	1.9913(10)	2.0057(14)		
Co/Ti–O(1)			2.083(8)/1.958(9)	2.070(5)/1.956(5)
Co/Ti–O(2)			2.022(9)/2.012(10)	2.025(8)/1.998(9)
Co/Ti–O(3)			2.087(8)/1.952(7)	2.097(5)/1.956(5)

[a]$\chi^2 = 1.239$; for $\lambda = 1.5403$ Å: w*R*p 4.87%, *R*p = 3.87%.
[b]Red $\chi^2 = 1.419$; for $\lambda = 1.5403$ Å: w*R*p 4.94%, *R*p = 3.98%.
[c]Red $\chi^2 = 1.033$; for $\lambda = 1.5403$ Å: w*R*p 6.69%, *R*p = 5.34%.
[d]Red $\chi^2 = 2.043$; for $\lambda = 1.5403$ Å: w*R*p 6.07%, *R*p = 4.86%; for $\lambda = 2.0788$ Å: w*R*p = 5.9%, *R*p = 4.44%.
*[Fraction Ti/ Fraction Co].

Table 2
Overall effective momement (p_{eff}), Weiss constant (θ_w), χ_0, magnetic transition temperature (T_M) in 1 T magnetic field

	p_{eff} (μ_B/f.u.)	θ_w (K)	χ_0 (emu/Oe f.u.)	T_M (K)
La_2NiVO_6	2.34	16.3	0.001	~2
La_2CoVO_6	5.34	−107.2	0	11.8
La_2CoTiO_6	4.45	−34.8	0.00075	14.8

tentatively attributed to the presence of sub-percentage levels of CoO. A very small nonlinearity at very low fields of the magnetization vs. field at 5 K (Inset Fig. 4) causes the data in Fig. 5 to not fall directly on top of each other.

La_2CoTiO_6 shows a sharp antiferromagnetic transition at 14.8 K as shown in the χ vs. T plot (Fig. 6 inset A). The magnetization is linear as a function of field (Fig. 6 inset B). A line fitted to the paramagnetic region of the $1/\chi$ vs. T

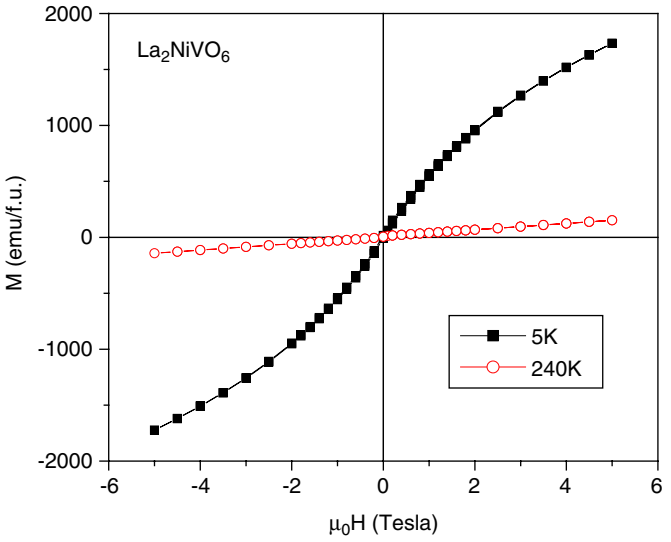

Fig. 2. M vs. H loop at 5 K (squares) and 240 K (circles) for La_2NiVO_6.

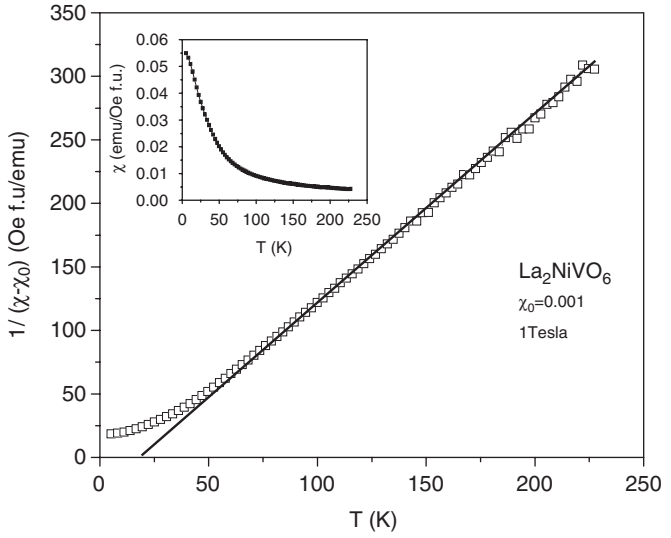

Fig. 3. $1/\chi$ vs. T La_2NiVO_6 with χ vs. T inset.

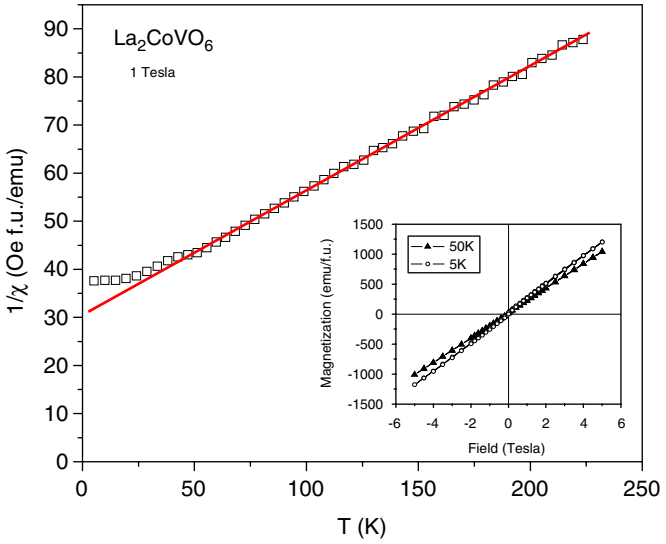

Fig. 4. $1/\chi$ vs. T La_2CoVO_6 with magnetization vs. field inset.

plot shows an θ_W intercept of -30.6 indicating antiferromagnetic interactions. The slope of the Curie–Weiss fit gives La_2CoTiO_6 an overall moment of $4.45\,\mu_B$/f.u., corresponding to the combined moments of Co^{2+} ($4.8\,\mu_B/Co^{2+}$ high spin) and Ti^{4+} ($0\,\mu_B/Ti^{4+}$) [20]. Neutron diffraction of La_2CoTiO_6, shown in Fig. 1C, confirmed the ordered state of the Co and Ti cations in the double perovskite structure, making the unit cell monoclinic ($P2_1/n$). This monoclinic structure is different from the previously reported orthorhombic structure [11]. Bond valence sums for the Co and Ti yielded effective charges of $+2.3$ and $+3.9$, respectively, consistent with the assignment of $2+$ and $4+$ oxidation states derived from the magnetic data.

Neutron powder diffraction of La_2CoTiO_6 was also performed at 4 K revealing a magnetic super cell (Fig. 1D). Magnetic peaks observed at 4 K, as shown in the inset of Fig. 1(D), can be indexed by a superstructure with lattice parameters $a \times 2b \times 2c$ and β, where a, b, c, and β are the nuclear structure unit cell constants. A magnetic structure model, as shown in Fig. 7, was tested to calculate the magnetic neutron powder diffraction pattern and gives a reasonably good fit to the observed intensities. In the calculation using the GSAS program we introduced a magnetic symmetry $P2/m'$ in which there are only four independent sites for magnetic cations (Co) in the magnetic unit cell at: $2i$ $(0,\frac{1}{4},0)$, $2k$ $(0,\frac{1}{4},\frac{1}{2})$, $2m$ $(\frac{1}{2},0,\frac{1}{4})$, and $2n$ $(\frac{1}{2},\frac{1}{2},\frac{1}{4})$. The magnetic symmetry $P2/m'$ allows moments parallel to the b direction for the $2i$ and $2k$ sites and moments are in the ac plane for the $2m$ and $2n$ sites. Calculations with moments parallel to the a direction result in no significantly different quality of fit from calculations with moments in the ac plane for the $2m$ and $2n$ sites, suggesting that the data are not able to determine the spin directions for these sites. The final refinement was performed by fixing the moments parallel to the a direction for the $2m$ and $2n$ sites. Neither moments nor improvement of fit were obtained by attempting to place moments on the Ti site. The lack of moment on this site is consistent with our Ti^{+4} d^0 assignment for the Ti based on the susceptibility data. Layers of spins, shown in Fig. 7, comprising chains of ferromagnetically aligned spins in the a direction, are antiferromagnetically aligned with adjacent spins in the b and c directions; spins on the $z = 0$ and $1/2$ layers are perpendicular to those spins in $z = 1/4$ and $3/4$ layers. This model differs from the previous report [12] in that the spins on the intermediate Co layers are perpendicular to those in the neighboring planes. Fig. 8 shows the $(0,\frac{1}{2},\frac{1}{2})$ magnetic peak intensity as a function of temperature. The solid curve is a fit to mean field theory to estimate an ordering temperature of 15.2(2) K, which is in good agreement with the magnetic susceptibility measurements (Fig. 6). T_N is somewhat lower for our material than has been reported previously $T_N \sim 20$ K [12].

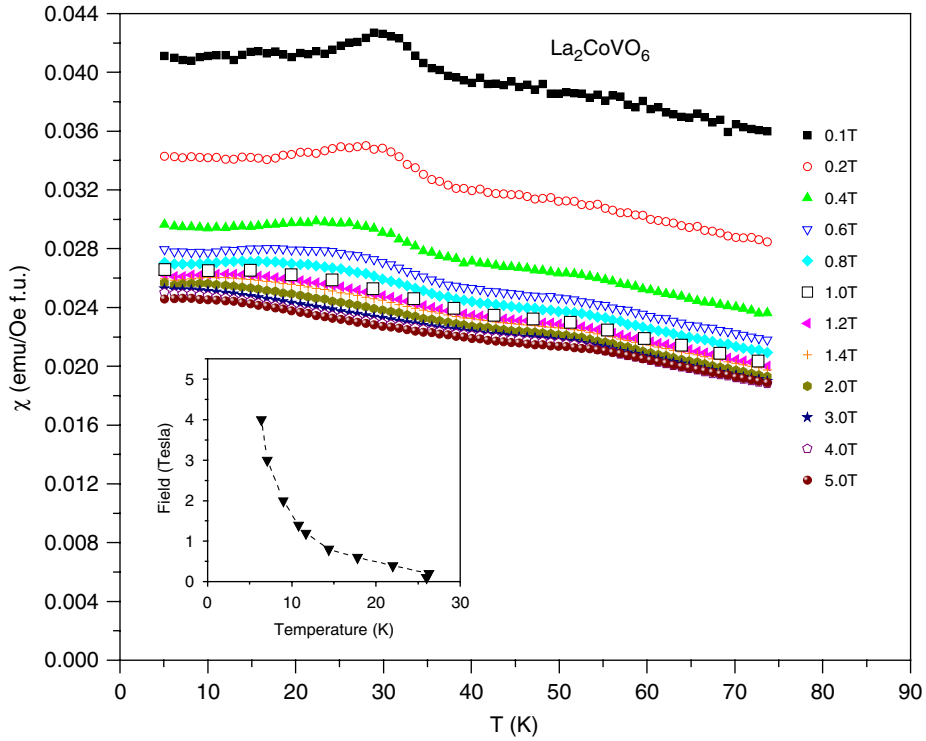

Fig. 5. χ vs. T La_2CoVO_6 with varying field from 0.1 T to 5 T with inset field vs. temperature identifying peak position.

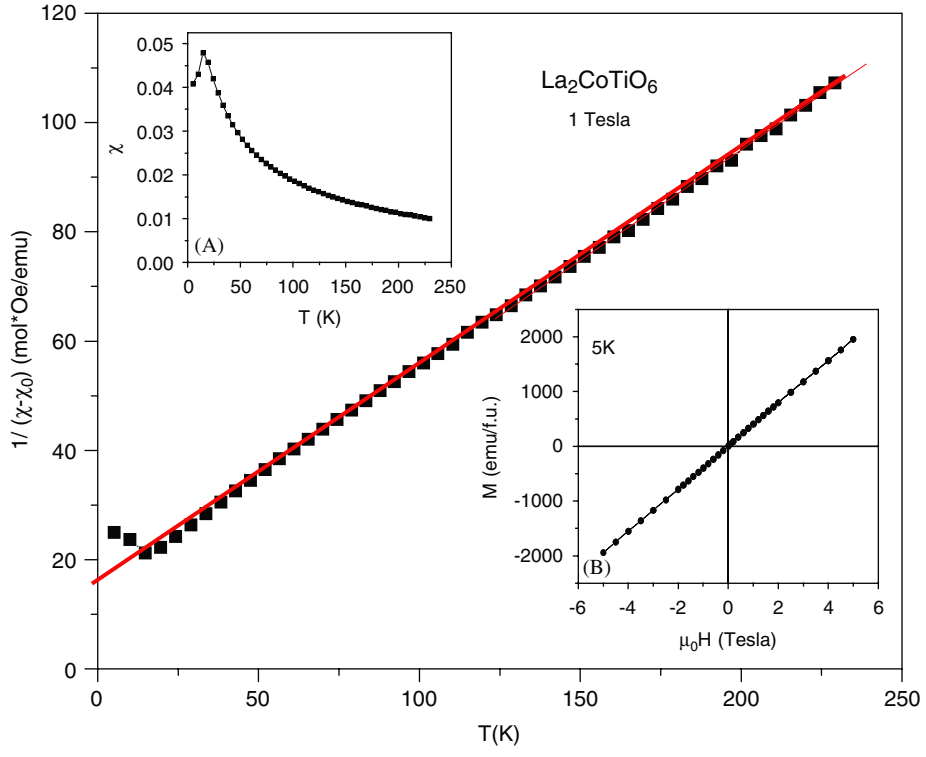

Fig. 6. $1/\chi$ vs. T La_2CoTiO_6 in a 1 T field. Inset A: χ vs. T in a 1 T field. Inset B: M vs. H loop at 5 K.

Temperature-dependent DC resistivity measurements showed that all three double perovskites display increasing resistivity with decreasing temperature (Fig. 9). La_2NiVO_6, La_2CoVO_6, and La_2CoTiO_6 are semiconducting with band gaps of 0.45, 0.41, and 1.02 eV, respectively. None of the compounds showed a significant change in resistivity when a field of 1 T was applied, indicating no magnetoresistive behavior.

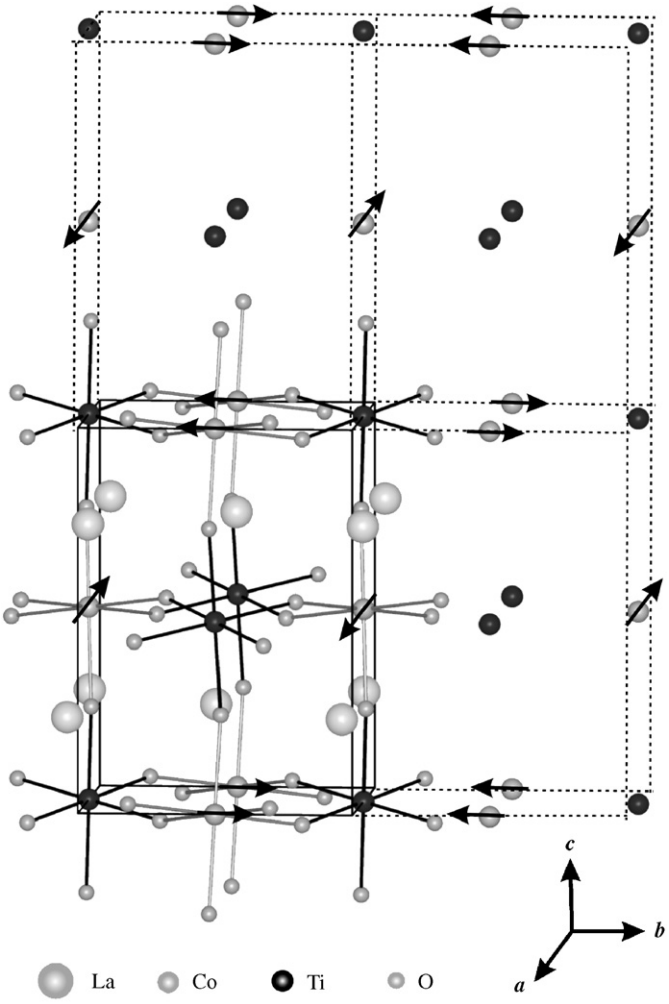

Fig. 7. Magnetic cell of La_2CoTiO_6 as determined by powder neutron diffraction at 4 K. Arrows are intended to show how the spins are oriented relative to each other in the $P2/m'$ magnetic symmetry.

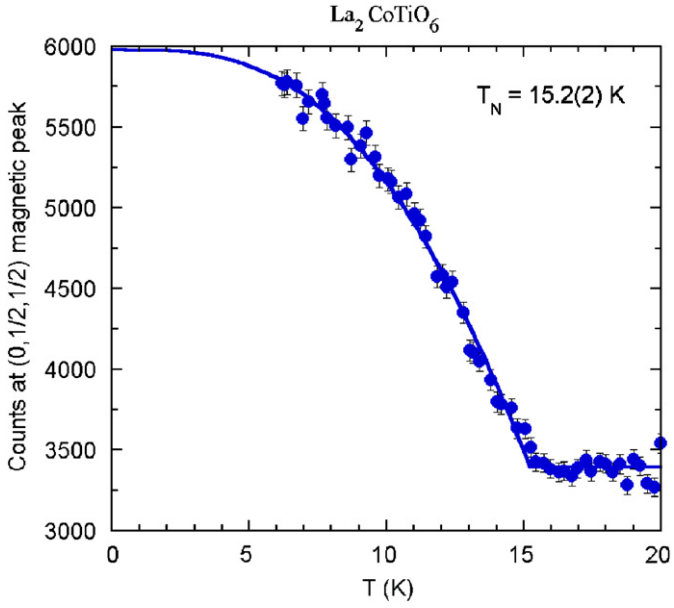

Fig. 8. Temperature dependent neutron diffraction measurements of the $(0,\frac{1}{2},\frac{1}{2})$ magnetic peak of La_2CoTiO_6. The solid curve is a mean-field fit to the data to estimate the Neél temperature.

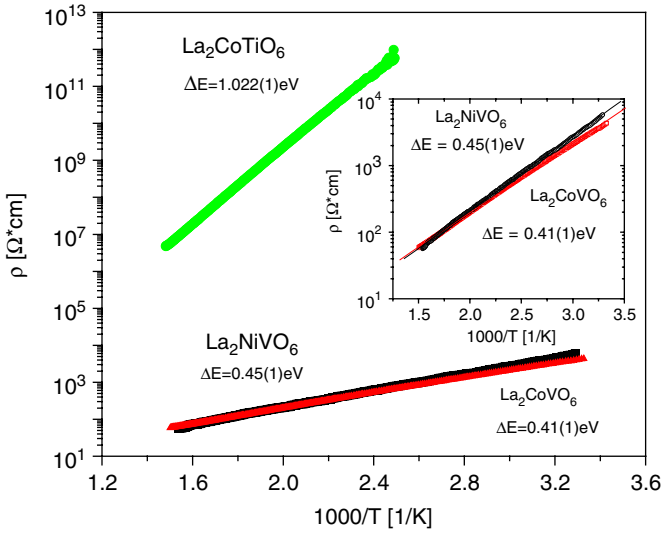

Fig. 9. Resistivity measurements ρ vs. $1000/T$ for La_2CoTiO_6, La_2NiVO_6, and La_2CoVO_6.

4. Conclusions

Two new double perovskites, La_2NiVO_6 and La_2CoVO_6, have been synthesized and characterized; La_2CoTiO_6 has also been investigated. La_2NiVO_6 and La_2CoVO_6 are orthorhombic perovskites, while La_2CoTiO_6 was found to be a monoclinic perovskite. Neutron diffraction indicates a disordered B sublattice for La_2NiVO_6 and La_2CoVO_6. La_2CoTiO_6 has an ordered B sublattice. La_2NiVO_6 shows Brillouin behavior at low temperatures, while La_2CoVO_6 and La_2CoTiO_6 show antiferromagnetic behavior. For La_2CoTiO_6, neutron diffraction reveals a long-range ordered antiferromagnetic arrangement of Co spins, while no significant moment was observed on the Ti sites. A simple model of antiferromagnetic spins is consistent with the data. The temperature dependence of the magnetic Bragg peak establishes a T_N of 15.2(2) K. Resistivity measurements of La_2NiVO_6, La_2CoVO_6, and La_2CoTiO_6 indicated that all three compounds are semiconductors. Future characterization of the low-temperature magnetic states of these materials may be of interest.

Acknowledgements

This work was supported by the NSF MRSEC program, Grant DMR – 0213706. Certain commercial material and equipment are identified in this report to describe the subject adequately. Such identification does not imply recommendation or endorsement by the NIST, nor does it

imply that the materials and equipment identified is necessarily the best available for the purpose.

References

[1] D.T. Marx, P.G. Radaelli, J.D. Jorgensen, et al., Phys. Rev. B. 46 (1992) 1144–1156.
[2] B.T. Cong, P.N.A. Huy, N.H. Long, J. Magn. Magn. Mater. 262 (2003) 437–440.
[3] B.D. Stojanovic, C. Javalekic, V. Vukotic, A.Z. Simoes, J.A. Varela, Ferroelectrics 319 (2005) 291–299.
[4] T. Kyomen, R. Yamazaki, M. Itoh, Phys. Rev. B. 68 (2003) 104416–104422.
[5] J.W.G. Bos, J.P. Attfield, Z. Anorg. Allg. Chem. 630 (2004) 2248–2252.
[6] P.M. Woodward, Acta Crystallogr. B 53 (1997) 32–43.
[7] R. Pinacca, M.C. Viola, J.C. Pedregosa, et al., Dalton Trans. 3 (2005) 447–451.
[8] M.T. Anderson, K.B. Greenwood, G.A. Taylor, K.R. Poeppelmeier, Prog. Solid State Chem. 22 (1993) 197–233.
[9] M.T. Anderson, K.R. Poeppelmeier, Chem. Mater. 2 (1991) 476–482.
[10] N.S. Rogado, J. Li, A.W. Sleight, M.A. Subramanian, Adv. Mater. 17 (2005) 2225–2227.
[11] N. Ramadass, J. Gopalakrishnan, M.V.C. Sastri, J. Inorg. Nucl. Chem. 40 (1978) 1453–1454.
[12] E. Rodriguez, M.L. Lopez, J. Campo, M.L. Veiga, C. Pico, J. Mater. Chem. 12 (2002) 2798–2802.
[13] R.S. Puche, J.L. Rodriguez, F. Fernandez, Inorg. Chim. Acta. 140 (1987) 151–153.
[14] D.J. Buttrey, Persp. Solid State Chem. (1995) 228–240.
[15] A. Nemudry, P. Rudolf, R. Schollhorn, Solid State Ionics 109 (1998) 213–222.
[16] A. Larson, R.B. Von Dreele, "General Structure Analysis System (GSAS)", Los Alamos National Laboratory Report LAUR 86-748, 2000.
[17] B.H. Toby, J. Appl. Crystallogr. 34 (2001) 210–213.
[18] A.M. Glazer, Acta Crystallogr. B 28 (1972) 3384–3392.
[19] R.H. Mitchell, Perovskites Modern and Ancient, Almay Press Inc., Ontario, Canada, 2002.
[20] N.W. Ashcroft, N.D. Mermin, Solid State Physics, Harcourt College Publishers, Fort Worth, 1976.